Tip-Enhanced Raman Spectroscopy (TERS)

Bruno Pettinger

Fritz Haber Institute of the Max Planck Society, Faradayweg 4–6, D-14195, Berlin, Germany
pettinger@fhi-berlin.mpg.de

1 Introduction

The understanding and knowledge of interfaces is of vital importance for science and technology. Yet, their investigation represents a great challenge still today. It becomes more and more important to achieve information at the level of individual structural blocks of the interfacial region. For the full understanding of interfacial processes, one needs both structural and chemical information at the atomic level. One example for developments in this direction is the advent of the scanning probe microscopies (SPM) [1, 2, 3, 4]. They permit monitoring of surface structures and even their changes in time with atomic resolution. While initially the SPM techniques could not reveal the chemical nature of atoms seen in SPM images, recent development, leading to ISTS (inelastic scanning tunneling spectroscopy), opens the view to the chemical nature of surface atoms and molecules [5, 6]. A major limitation in these experiments is the need for UHV conditions and cryogenic temperatures for the necessary stability of the sample–probe arrangement [6].

IST spectroscopy belongs to the class of vibronic spectroscopies, as well as Raman or infrared spectroscopy. The latter two are optical spectroscopies and provide information on the chemical nature of the investigated species. However, the information (spectrum) is usually averaged over a large ensemble and can, therefore, contain only a certain amount of structural information. While initially Raman spectroscopy was not considered to be sensitive enough to become a suitable tool for interfacial studies (in contrast to infrared spectroscopy), detections and developments in the last decades and even more in the last several years has turned this picture upside down: Due to the availability of huge surface enhancement(s), Raman spectroscopy belongs to the most sensitive vibronic spectroscopies today[1] [7, 8, 9, 10, 11].

The field of surface-enhanced Raman spectroscopy (SERS) started in 1973 with the famous papers of *Fleischmann* et al. [12] and *Jeanmarie* and *Van Duyne* [13], giving rise to more than 4000 papers in the following decades. Most recent key words for intriguing approaches in the SERS field are "hot

[1] Certainly, this will hold also for the next several years. The sensitivity of STS is similar; however, its spectral resolution is comparatively poor.

K. Kneipp, M. Moskovits, H. Kneipp (Eds.): Surface-Enhanced Raman Scattering – Physics and Applications, Topics Appl. Phys. **103**, 217–240 (2006)

spots" and "single-molecule SERS" (this book will contain a number of contributions for both of these hot fields).

It is not necessary to present the case of surface-enhanced Raman spectroscopy in detail in this Chapter. What we would like to address here is the general problem of SERS: (Large) enhancements for adsorbates are only found for the coinage metals (copper, silver and gold) and only if these metals have nonplanar surfaces[2]. There is a commonly accepted explanation for these observations: One of the enhancement mechanisms (denoted as *electromagnetic enhancement*) is correlated with the excitation of surface plasmons within small metal structures [14]. Excited surface plasmons are associated with collective electron oscillations in the surface region; they create a localized electromagnetic field with a field strength often much higher than that of the incident wave. In a sense, the nonplanar surface structures act as an antenna for the amplification of the incident *and* radiated electromagnetic fields. The second enhancement mechanism is denoted as the *chemical enhancement* mechanism and is often considered as a kind of resonance Raman enhancement for adsorbate–substrate complexes that provide new or modified orbitals for (pre-)resonant excitation of the Raman processes [15].

The general obstacle for SERS is that adsorption or chemisorption, electromagnetic and chemical enhancement are strongly interconnected. Adsorption and chemisorption can change the (local) surface structure, with impacts on the chemical, but also on the electromagnetic enhancement (particularly if very small structures in the nanometer regime are responsible for huge enhancements). In recent years, a powerful concept was proposed: The concept of a few "hot spots" making up most of the SER signal while the rest of the surface is comparatively SERS inactive [16, 17, 18]. Consensus has been reached that nanostructures or nanoparticles approaching each other very closely provide the scenario for such hot spots: The interstitial region between the particles provide new, very localized modes of surface plasmons with extraordinary field strengths. Hence, these regions produce the strongest enhancements. The field of *single-molecule SERS* is based on this fact (see other Chapters in this book) [14]. In a sense, the lightning-rod effect [19] can be considered as a precursor of the concept of hot spots [20], as both concepts describe a sort of focusing of field energy into narrow spatial regions.

As a consequence of the hot-spot concept, one could have considered to create a single hot spot, for example, by moving a sharp protrusion or a tip made of silver or gold towards the sample under investigation. Illuminating the whole unit should also produce enhanced Raman scattering. In contrast, the development of SERS towards tip-enhanced Raman spectroscopy (TERS) went along a different route (see the next Chapter). In fact, the use of the hot spot in terms of an external device was developed in the SNOM field (scanning

[2] Periodic and nonperiodic structures support SERS; to the latter belong roughened surfaces and fractal structures. SERS is also observed for small single spheres as well as for aggregated nanoparticles.

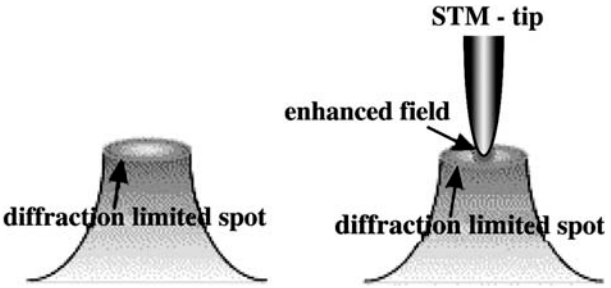

Fig. 1. Conceptual figure of (**a**) normal micro-Raman detection (far-field detection) as compared to (**b**) near-field Raman detection by a metallic probe tip. (Reprinted with permission from [21])

near-field optical microscopy) and was first denoted as apertureless SNOM (a-SNOM).

Nevertheless, once the TERS approach had been born, it was quickly understood that TERS belonged to one of the most intriguing developments in optical spectroscopy [21, 22, 23, 24, 25, 26, 27, 28, 29, 30, 31, 32, 33, 34]. It uses an illuminated scanning probe tip of a scanning probe device to greatly enhance the Raman scattering from the sample underneath the tip. In this way, Raman spectroscopy and scanning probe microscopy are married, forming a new spectroscopic–microscopic tool with hitherto unprecedented spectroscopic and spatial sensitivity. Suitable tips are either silverized AFM tips or STM tips made of a thin wire of silver or gold. As illustrated in Fig. 1, upon illumination of the tip with a sufficiently focused laser beam, localized surface plasmons are excited mainly near the tip apex leading to an enhanced electromagnetic (em) field in a very small region near or underneath the tip apex. It has a radius r_{tip} that is usually much smaller than the radius of the focal region r_{focus}. In TERS experiments, one can measure both the Raman scattering intensities in the absence ($I_{\mathrm{RS,\ tip\ retracted}}$) and in the presence of the tip ($I_{\mathrm{RS,\ tip\ down}}$). The ratio of the two intensities is often $\gg 1$, but in many cases < 100. Thus, the TERS enhancement may reach values between two and four orders of magnitude, which is sufficient to monitor TERS for strong Raman scatterers such as dyes. Compared to theoretically predicted enhancement factors of more than 10^{10} and in view of giant enhancements reported for single-molecule SERS ($\geq 10^{14}$), TERS shows a rather moderate enhancement range. Obviously, one can expect much higher TERS signals if the experimental conditions are improved with respect to more efficient excitation and radiation of localized surface plasmons.

In this contribution, we would like to sketch the developments in the field of TERS from 2000 to 2005. During these years, a number of advances have taken place. A striking one is an enhancement three or four orders of magnitude higher than in the initial reports that allows monitoring of even small molecules adsorbed at single-crystalline samples.

The present chapter is organized as follows: After this introduction, also briefly sketching SERS and the principles of TERS (Sect. 1), Sect. 2 will report a number of TERS studies, including our own recent investigations with single-crystalline substrates. Section 3 gives a short outlook.

2 TERS Results

Before beginning with the reports on tip-enhanced Raman scattering, we would like to comment on surface-enhanced resonance Raman scattering (SERRS), relevant for both the field of single-molecule SERS and TERS, when using strong Raman scatterers such as dyes.

2.1 Remarks on SERRS

Particularly huge surface enhancements are observed for dye molecules that show a strong absorption in the visible frequency regime [35, 36, 37], among them rhodamine 6g or crystal violet. Adsorbed, for example, at aggregated Ag colloids, they show extremely large total enhancements [38, 39, 40, 41]. In such systems, the differential cross sections for SERRS can easily be measured to be around $(\mathrm{d}\sigma/\,\mathrm{d}\Omega)_{\mathrm{SERRS}} \simeq 10^{-18}\,\mathrm{cm}^2 \cdot \mathrm{sr}^{-1}$ for individual Raman lines [39, 40, 41]. The total Raman cross section including an intense SERS background amounts to about $\sigma \simeq 10^{-16}\,\mathrm{cm}^2$. It is substantially more difficult, however, to determine the actual enhancement factors directly, because the intense fluorescence obstructs any resonance Raman measurement of the free rhodamine 6g molecules excited around 514.5 nm. Fortunately, the differential cross section for normal and resonance Raman scattering (RRS) of these molecules can be roughly estimated. As is well known, in the absence of optical resonance, the polarizability and, hence, the differential cross section scale linearly with the molecular volume or the number of electrons in a molecule. Thus, based on the low cross section of simple gases [42], the dye's cross section for normal Raman scattering (NRS) may be estimated as $(\mathrm{d}\sigma/\,\mathrm{d}\Omega)_{\mathrm{NRS}} \simeq 10^{-28}\,\mathrm{cm}^2 \cdot \mathrm{sr}^{-1}$. Obviously, the total enhancement factor (surface × resonance Raman enhancement) is $F_{\mathrm{SERRS}} \approx 10^{10}$. For the $1184\,\mathrm{cm}^{-1}$ vibrational mode of rhodamine 6G adsorbed at glassy carbon (for this system no electromagnetic (em) enhancement is expected [43]), *Kagan* and *McCreery* reported a differential cross section of $(\mathrm{d}\sigma/\,\mathrm{d}\Omega)_{\mathrm{RRS}} \simeq 10^{-25}\,\mathrm{cm}^2 \cdot \mathrm{sr}^{-1}$. This indicates the presence of a classical RRS enhancement of 10^3 in accordance with the usually expected 10^2- to 10^5-fold resonance Raman enhancement for free dye molecules [44]. Consequently, for the colloidal solutions considered here, one estimates the (average) em enhancement factor as about 10^7. If one takes into account that only a small fraction of dye molecules ($\sim 1\,\%$) is adsorbed within the interstitial volume of two particles that presumably is the location of giant field enhancement, the em enhancement factor is "only" around 10^9. Although

the cross sections presented above are comparable to these recently reported in the field of single-molecule SERS, the estimated em enhancement ($\sim 10^9$) is rather conservative compared to values reportedly one to four orders of magnitude higher [8, 14, 45]. Please note that in the above estimate, the contribution of resonance Raman processes to the total enhancement is most likely underestimated. Yet, the remaining electromagnetic enhancement of around 10^9 remains huge. Important in this context is that localized surface-plasmon (LSP) resonances and a few (or even single), light-absorbing dye molecules adsorbed in the high-field zone must show mutual interactions: For dyes showing bleaching behavior such as rhodamine 6g excited at 488 nm or 514.5 nm, the enhanced field provided by the LSP should result in an enhanced rapid bleaching rate. In turn, the higher the field enhancement due to LSP resonances, the more sensitive these resonances must respond to light-absorbing species. These effects seem to be (nearly) absent in the field of single-molecule SERS, while a few reports (in somewhat different fields) show a decrease of the enhancement with increasing dye coverage for colloidal systems and a rapid dye bleaching in the case of TERS (this effect will be addressed below).

2.2 Initial Steps in TERS

The Zenobi group put substantial effort into improving the SNOM approach and adapting Raman spectroscopy to it. One key problem has been, and still is, the insensitivity of the tapered fiber tip that reduces the transmission of both the incident and scattered light. Although the choice of a suitable tip shape and its metallization have substantially improved the throughput of light [46], there still is an unavoidable limitation to this technique: The higher the required spatial resolution of this technique, the narrower the aperture of the tip has to be; this, however, reduces the field strength and the area from which the signal is collected. In other words, the SNOM resolution cannot be much better than 50 nm. To overcome this limitation, *Stöckle* et al. [22] designed an apertureless SNOM (a-SNOM) by using a silverized AFM tip with a granular silver film of about 20 nm thickness. Under illumination of the AFM tip, one of the particles at the tip apex acts as an antenna for the incident light and permits the excitation of surface plasmons. This leads to an increased local electromagnetic field. If the illuminated AFM tip is in (close) contact with the sample, an enhanced light scattering is observed. In fact, *Stöckle* et al. [22] reported a large gain in the Raman scattering intensity[3] for a dye film (brilliant cresyl blue) deposited on a glass substrate if a metalized AFM tip is set to close contact with this sample. Figure 2 reproduces the upper part of Fig. 1 in [22]. The two spectra, denoted as curves *a* and *b*, refer

[3] As indicated by the insert in Fig. 2, an inverted microscope objective has been used to focus the laser beam through the glass slide covered by a dye film onto the AFM tip.

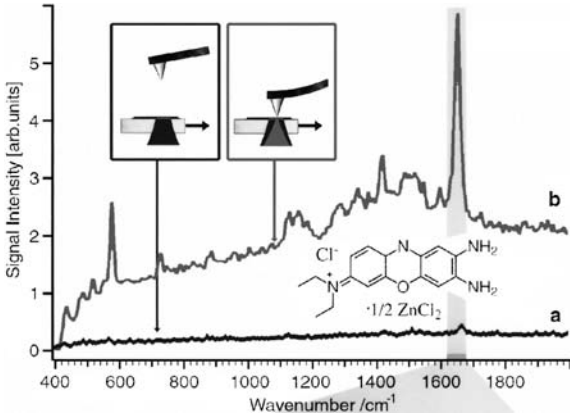

Fig. 2. Tip-enhanced Raman spectra of brilliant cresyl blue (BCB) dispersed on a glass support and measured with a silver-coated AFM probe. The two Raman spectra were measured with the tip retracted from the sample (**a**) and with the tip in contact with the sample (**b**), respectively. (Reprinted with permission from [22])

to the tip retracted from and in contact mode with the sample, respectively. The authors report a more than 30-fold net increase[4] of the Raman signal by the tip. Taking into account the small area of the enhanced field underneath the tip of less than 50 nm in diameter, a 2000-fold enhancement of Raman scattering in the vicinity of the tip has been deduced. Similar effects were reported for C_{60} molecules and an electrochemically etched Au tip with an apex of 20 nm in diameter (this tip is mounted in a shear-force setup). In addition, the authors also illustrated that the spatial resolution of this approach was about 55 nm [22].

A similar approach was presented by *Nieman* et al. [26]. They used an illuminated AFM tip covered with a 100 nm gold film to enhance Raman scattering from samples of polydiacetylene para-toluene sulfonate and two-photon-induced fluorescence from crystallites of coumarin I dye. An example of the latter effect is shown in Fig. 3. In this experiment, coumarin I was dried on a coverslip. A mode-locked Ti:Sa laser served as the excitation source with a 200 fs pulse width, an excitation line around 790 nm and a power of less than 100 μW. In order to ensure that a tip enhancement occurs, the fluorescence signals (recorded in the wavelength region of 535 nm to 565 nm) were recorded for polarizations with major components perpendicular or parallel to the tip axis.

According to Fig. 3, the fluorescence signal for parallel polarization is about twice as large as for the perpendicular polarization. This suggests

[4] By net increase we mean the n-fold ($f_{n\text{gain}}$) increase of the overall Raman signal in the presence of the tip compared with the Raman intensity observed in the absence or retraction position of the tip.

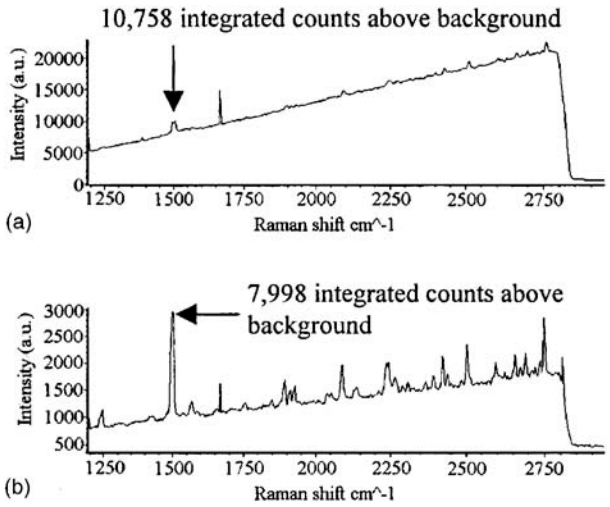

Fig. 3. Fluorescence spectra taken with a LN–CCD camera in the reflection path with an exposure time of 2 min. During acquisition, the gold-coated tip was imaging in noncontact mode with a scan rate of 0.3 Hz over a 5 μm × 5 μm area. (**a**) Incident beam polarization perpendicular to the plane of the tip. (**b**) Incident beam polarization parallel to the plane of the tip. The integrated peak intensity from polarization parallel to the plane of the tip is a factor 2.4 larger than from polarization perpendicular to the plane of the tip. (Reprinted with permission from [26])

a strong enhancement of the two-photon-induced fluorescence by the gold-covered AFM tip, because there is no influence of the polarization on the fluorescence signal in the absence of the tip. The authors observed images produced by the near-field of the illuminated tip with a resolution of about 100 nm.

Hayazawa compared far-field- and near-field-excited Raman scattering for rhodamine 6g on a silver-island film. A silverized cantilever tip was used with a coating thickness of 40 nm. The Ag-island film was evaporated on a thin glass slide that was brought into optical contact with the objective (NA = 1.4) using an immersion oil. Both the excitation of the Raman scattering and the recording of the emitted radiation were performed with the same objective. Figure 4 shows the near-field spectrum of rhodamine 6g, denoted as spectrum (a), obtained as the difference between spectra recorded in the presence and absence of the AFM tip. For comparison, a spectrum is shown where a pure cantilever is used.

This shows that only the thin silver film, i.e., only one of the silver particles at the tip apex, generates the enhancement again by the excitation of localized surface plasmons that produce an enhanced field near the tip apex. Hayazawa et al. estimate a 40-fold enhancement for Raman scattering. It is noteworthy that the dye on the silver-island film already showed a surface

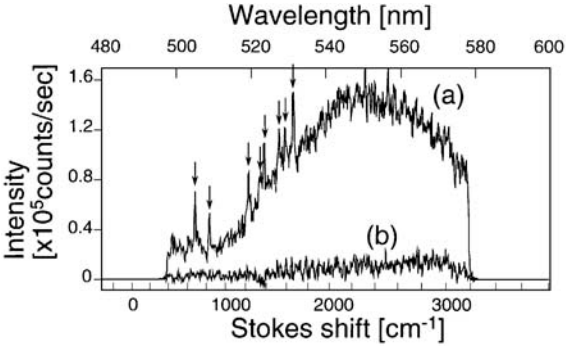

Fig. 4. (a) Near-field spectrum corresponding to the difference of spectra with and without a cantilever at a tip–sample distance of 0 nm. (**b**) The same as (**a**), but with a silicon cantilever. The laser power is 0.5 mW and the exposure time is 5 s. (Reprinted with permission from [24])

enhancement; in the presence of the tip, a further 40-fold enhancement could be achieved. In a later paper, Hayazawa et al. presented an interesting experiment: Two different dyes, rhodamine 6g and crystal violet, were deposited on a substrate and near-field Raman images and topographic AFM images were recorded. These images are reproduced in Fig. 5, each showing an area of $1\,\mu m \times 1\,\mu m$. To identify the two dye molecules and to differentiate between them, two characteristic Raman bands were used: 1. The $607\,cm^{-1}$ line of the C–C–C in-plane bending mode of rhodamine 6g for Fig. 5a, and 2. the $908\,cm^{-1}$ line of the C–H out-of-plane bending mode of crystal violet for Fig. 5b. A third line, the C–H inplane bending mode of crystal violet at $1172\,cm^{-1}$, is used to record another near-field Raman image (Fig. 5c) of the crystal violet distribution on the substrate. The fourth figure (Fig. 5d) shows a topologic AFM image that was simultaneously recorded with the image of Fig. 5a.

By using the different Stokes-shifted Raman lines, the distribution of the two molecules within the imaged area can be monitored, which is impossible with the topological image [21]. Although the resolution and the differentiation between the two molecules are limited, these results show the high potential of TERS for providing chemical information about adsorbed species with a spatial resolution in the nanometer region.

As shown above, in the first TERS studies, strong Raman scatterers were studied such as brilliant cresyl blue (BCB), fullerenes, sulfur layers or rhodamine 6g and crystal violet. In these cases, the high Raman cross sections allowed measurements of both the Raman scattering in the absence and in the presence of the tip. From the ratio of these signals, one can evaluate the net gain observed in these experiments. In the publications on TERS between 2000 and 2003, the reported net gains range between 1.5 and 40, which is associated with a local enhancement of Raman scattering by about

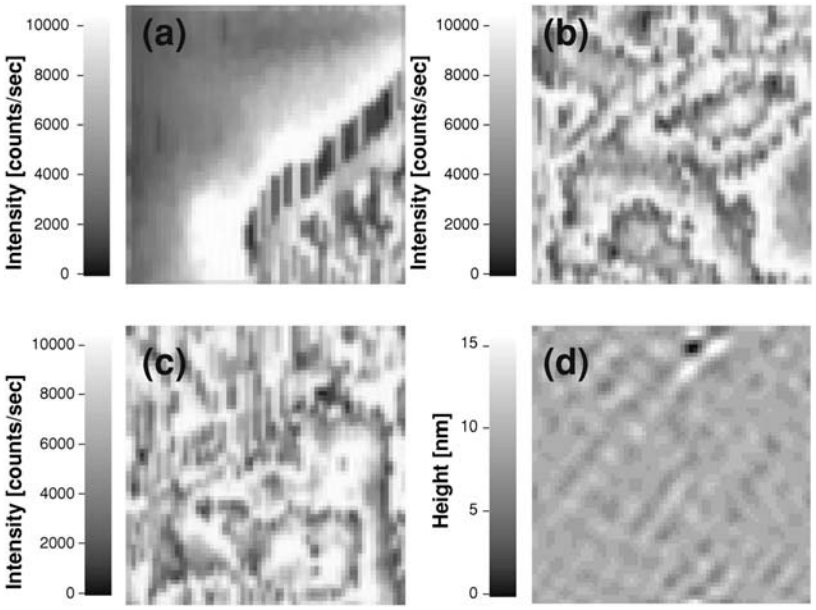

Fig. 5. Near-field Raman images obtained at (**a**) $607\,\mathrm{cm}^{-1}$ for the C–C–C inplane bending mode of rhodamine 6g, (**b**) $908\,\mathrm{cm}^{-1}$ for the C–H out-of-plane bending mode of crystal violet, and (**c**) $1172\,\mathrm{cm}^{-1}$ for the C–H inplane bending mode of crystal violet. (**d**) is the corresponding topologic image. Recording time: 10 min for one image consisting of 64 by 64 pixels covering a $1\,\mu\mathrm{m} \times 1\,\mu\mathrm{m}$ scanning area. (Reprinted with permission from [21])

two to four orders of magnitude. In most cases, AFM tips covered with Ag or Au films were used for the TERS experiments. A wide variety of samples indicate the general applicability of this approach. Let me just list a few examples: Thin BCB films on glass slides [22], or C_{60} molecules on glass or quartz slides [22, 23], thin sulfur films on quartz [23], rhodamine 6g on a thin Ag film [21,24], tip-induced SERS of a polydiacetylene (PDA–PTS) [26], diamond particles on glass [47], single-walled carbon nanotubes on glass [28].

STM devices implemented for TERS are less common, probably for one reason: One needs a conductive surface, and, hence, TERS using an STM device seems to be a less-general approach. However, this approach has its own merits: It provides an excellent distance control, and, if a suitable metal substrate is used, it has a higher spatial resolution according to theory. An additional advantage is a very efficient fluorescence quenching for fluorescent species adsorbed at a metal substrate. This latter property permits us to work even in spectral regions that otherwise would be inaccessible due to an overwhelming fluorescence. *Pettinger* et al. [25, 27] reported on TERS for BCB adsorbed on a thin, smooth gold film and exciting the Raman process

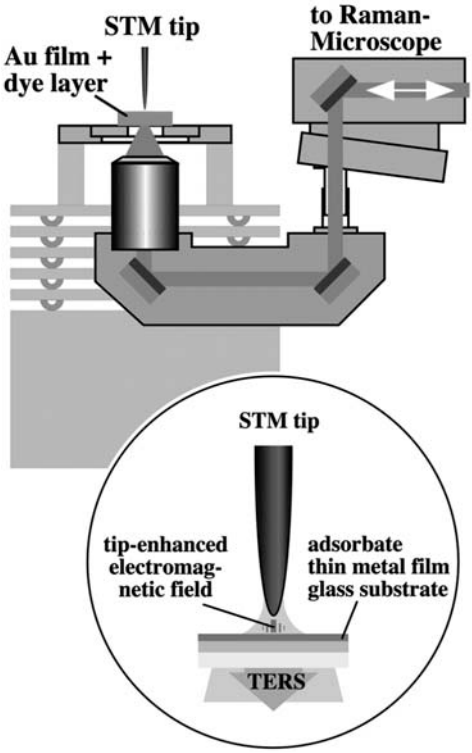

Fig. 6. Experimental scheme of the TERS experiment. Please note that the laser beam is passed through the thin metal film to excite the optical modes of the tip–metal junction. Light scattered by the adsorbate is collected in the backscattering mode and also passed through the thin metal film. (Reproduced with permission from [27])

with a He–Ne laser line at 632.8 nm. Figure 6 shows the TERS setup using the inverted microscope approach.

The Raman system is a LabRam1000 from Dilor that consists of a microscope stage attached to a Raman spectrograph. A U-turn inverts the light beam that is then focused on the sample through a glass slide and through a thin metal film by an inverted microscope objective of 50× or 100× magnification. The scattered light is collected in the backscattering mode. It is then passed through a cinematic notch filter system to the spectrograph and dispersed on a liquid-nitrogen-cooled CCD camera. An in-house-built STM is mounted on an x–y-stage driven by piezoelements in order to bring the tunneling tip into the illuminated focal spot. During the experiments, the bias voltage is kept at 50 mV with a constant tunneling current of 1 nA. In these TERS experiments, silver tips were made from 0.25 mm silver wire (99.998 % purity, Alfa Aesar) by electrochemical etching in perchloric acid, ethanol and

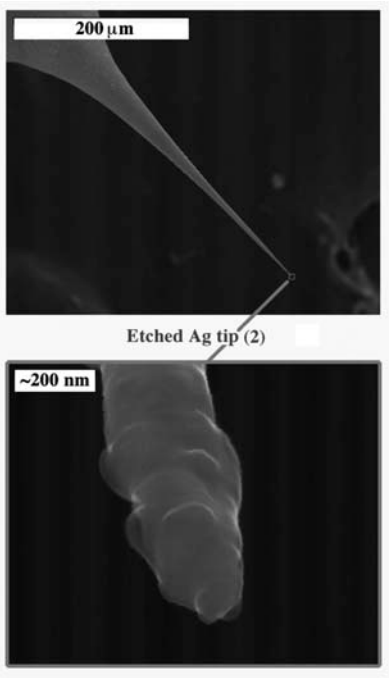

Fig. 7. Images of an electrochemically etched silver tip. The etching procedure is described in the text. (Reprinted with permission from [27])

water (Streuers) using a gold ring as a counter electrode that results in tip radii of about 100 nm (see Fig. 7) [27].

As seen from the fluorescence spectrum in Fig. 8 measured for a BCB layer deposited on glass, the laser line lies within the fluorescence region of this dye (its maximum is around 660 nm). If the dye is adsorbed on a thin Au film (12 nm evaporated on a glass slide) in monolayer or submonolayer quantities, no fluorescence is observable, but Raman scattering is seen (see curve 1 in Fig. 9). This Raman scattering is rather weak for two reasons: The coverage is a monolayer or less, and the gain in signal provided by the resonance Raman effect is about three orders of magnitude. Therefore, only the strongest peak (here at about 540 cm^{-1} due to the excitation in the red at 633 nm) is discernible while the other BCB bands are more or less hidden in the noise. If, however, the STM tip is moved into the laser focus and into a tunneling position, a significant rise in the overall Raman signal is observed with a net increase of about $f_{n\text{gain}} \sim 16$ for all Raman lines (curve 2 in Fig. 9).

Based on a tip radius of about 80 nm and a focal radius of 500 nm (100× magnification), the TERS enhancement in these experiments amounts to about three orders of magnitude ($f_{\text{TERS}} = f_{n\text{gain}} * (r_{\text{focus}}/r_{\text{tip}})^2 \sim 630$).

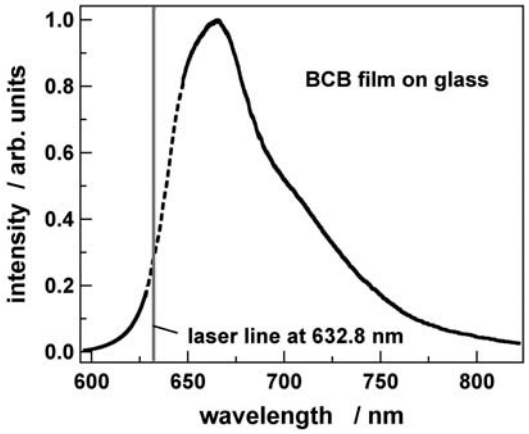

Fig. 8. Fluorescence spectrum of brilliant cresyl blue, recorded in backscattering mode. (Reprinted with permission from [27])

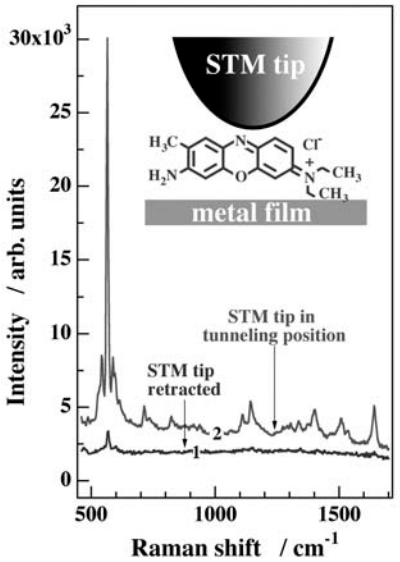

Fig. 9. Resonance Raman scattering and TERS for brilliant cresyl blue (BCB) on a smooth gold film (thickness $d = 12\,\text{nm}$). (Reprinted with permission from [27])

The weak points of these initial TERS studies are: 1. The polarization of the laser light perpendicular to the tip axis (which is less efficient for surface-plasmon excitations)[5], 2. both the incident and scattered light having to pass the metal film, 3. the adsorbates are possibly not in a favorable adsorption geometry, and 4. tips made of silver, because they are not inert enough, as long as one works in air.[6]

2.3 Towards Higher Efficiencies in TERS

The above-discussed point forced us to also test tips made of gold, a material well known for its inertness.[7] In our experiments, Au tips yielded similar enhancements as Ag tips. However, SEM images showed that electrochemically etched tips were often very rough. The experience with SERS tells us, however, that roughened tip surfaces provide a number of locations for local surface-plasmon (LSP) excitations with varying enhancements, but without any guarantee that the one particle at the end of tip apex is the most suitable one for TERS. In contrast to that, the presumably optimal and single location of LSP excitation would be the small tip apex of a smooth tip with a sufficiently narrow tip cone. Indeed, theoretical studies indicate huge enhancements for rather narrow tips, with field enhancements of 300 to more than 1000. According to the famous g^4 law, this should lead to about a 10^{10}- to more than 10^{12}-fold TERS enhancements [48, 49]. Obviously, there is a large gap between the theoretically predicted and the (so far) experimentally reported TERS enhancements of 10^4. To close this gap, tips with improved performance are needed. In other words, we were searching for a tip preparation procedure that leads to sharp tips with a smooth surface. In a detailed study, *Ren* et a. [34] developed an electrochemical etching procedure that meets the requirement just mentioned. It is a rather simple procedure that requires only a beaker filled with a 1 : 1 mixture of fuming HCl and ethanol as shown in Fig. 10. The Au wire is dipped into the etching solution with an immersion length of the wire of 2 mm to 3 mm. The etching is performed by applying a potential of 2.4 V between the Au wire and a gold ring counter electrode [34].

It is important that the mixture of fuming HCl and ethanol leads to a reduction of bubbling in the solution, and the high electrode potential to a fast and more homogeneous removal of material. For both parameters, the mixing and the electrode potential, optimal conditions will lead to sharp and smooth tips. In Fig. 11, a series of SEM images is shown that illustrates

[5] This point holds also for AFM-based experiments if the illumination occurs along the tip axis.

[6] Silver exposed to ambient conditions will quickly be contaminated by impurities. In addition, it is continuously oxidized even down to bulk silver layers.

[7] From the ambient this is still a problem, though gold is much more inert than silver; therefore, we seldom use tips for a time longer than one day.

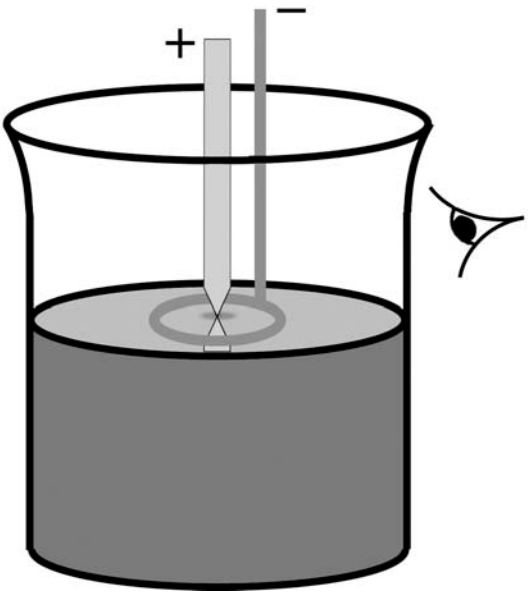

Fig. 10. Scheme of electrochemical etching of gold tips. (Reprinted with permission from [34])

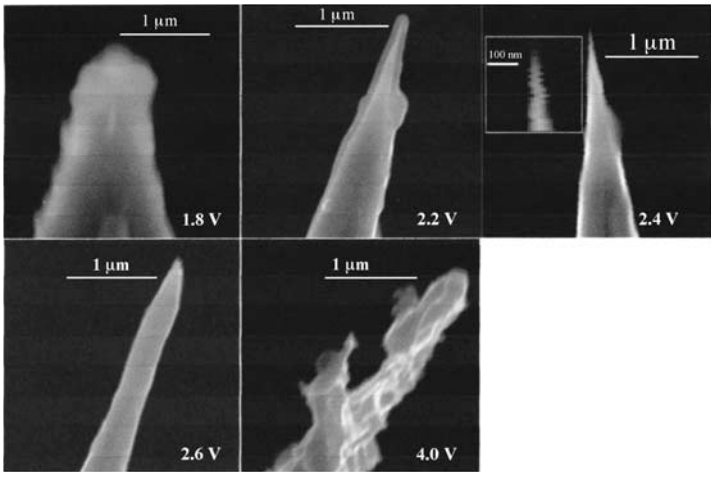

Fig. 11. Images of gold tips for different electrochemical etching potential. (Reprinted with permission from [34])

remarkable changes in surface structures with a varying electrode potential. Optimal smoothness is found for a potential of 2.4 V.

For the desired etching, it is also advantageous that a meniscus forms between the Au wire and electrolyte that leads to the conical form of the etched tips. If the wire is getting too thin to carry its lower part, it will break and the rest of the wire will drop. At this stage the electric circuit was cut off manually in earlier experiments. Now, an electronic device cuts off the electric circuit, when a preset current threshold is reached. Under these conditions, Au tips with apex radii of 20 nm to 30 nm can be produced routinely.

In our view, another important improvement was the use of side illumination of the tip. In this way, the disadvantageous polarization of the inverse-microscope approach, where the laser beam and the backscattered light propagate along the tip axis, can be avoided. Because the main polarization is oriented perpendicularly to the tip axis, the LSP modes will be less efficiently excited. In addition, the recording of the scattered light is inefficient, as its emission cone is not centered in the backscattering direction [49, 50].

As depicted in Fig. 12, the side-illumination approach means the redirection of the incident laser beam to an angle of 60° relative to the surface normal and the focusing onto the sample by a correspondingly oriented objective. The scattered light is collected by the same objective in the backscattering mode; it sends the scattered radiation backwards to the spectrograph. In this configuration, a strong polarization component exists parallel to the tip axis; also, the radiation of the scattered light is centered along the backscattering direction, and, last but not least, massive, opaque samples can be used. Together with suitable tips, this experimental configuration supports both an efficient excitation of localized surface plasmons (LSP) and an optimal recording of inelastically scattered light.

Malachite green isothiocyanate (MGITC) chemisorbed at a smooth Au(111) surface was chosen as a test system together with a Au tip. The adsorbate under investigation is located in the cavity formed between the tip and the Au(111) surface and is exposed to the field enhancement upon illumination. Before the experiment, the Au(111) sample was flame-annealed, which leads to a well-defined surface structure and removes contaminations [51]. In order to form a submonolayer of dye molecules, the crystal was wetted with a droplet of a 10^{-6} M ethanolic MGITC solution and dried. During the drying procedure, the dye molecules that came into contact with the metal surface were chemisorbed irreversibly through their sulfur atoms. In this way, a self-assembled (sub-)monolayer was formed. Subsequently, the sample was washed with copious amounts of ethanol to remove all molecules not directly bound to the gold substrate.

TERS experiments with MGITC on Au(111) generally showed a bleaching behavior. This means that the TER signals decay under illumination at a rate that depends on the incident laser intensity. Figure 13 shows a 3D plot of the TER intensity vs. Raman shift and vs. total time. To avoid too fast a bleaching, the laser power was reduced to 0.5 mW. Yet, the TER intensities

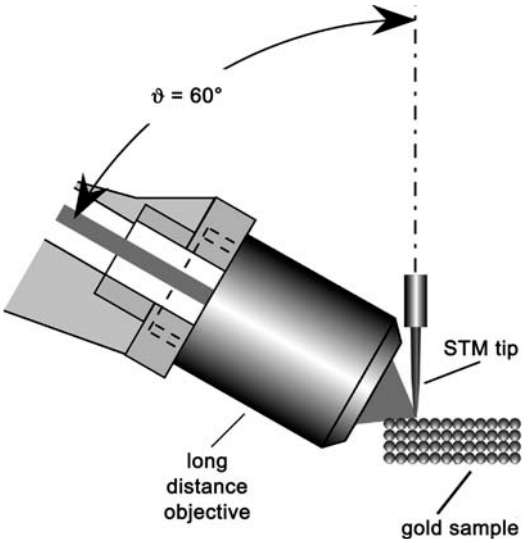

Fig. 12. 60° set up for TERS. Olympus long-distance objective: 50× magnification, NA 0.5. He–Ne laser: 5 mW at the sample, $\lambda_{ex} = 632.8$ nm. (Reprinted with permission from [33])

in Fig. 13 drop quickly within a few seconds and then level off at a slower rate.

For a deeper understanding of the bleaching let us investigate the time dependence of the 1618 cm^{-1} band. It shows the fastest intensity decay: After 70 s of illumination, it has only $\frac{1}{20}$ of its initial value, whereas the band at 1584 cm^{-1} still exhibits 25 % of its initial level. Obviously, the 1618 cm^{-1} band is more affected by the photofragmentation and growing disorder during the photobleaching than the 1584 cm^{-1} band [52]. Moreover, because of the sensitivity of the bleaching to the (local) intensity, differences in the bleaching rates for the cases "tip retracted" and "tip tunneling" can be related directly to the corresponding different (local) intensities. In other words, the ratio of the bleaching time constants represents a measure of the local field enhancement.

Figure 14 shows the time dependence of the resonance Raman intensity of the 1618 cm^{-1} band (no tip, hence, no field enhancement is present). The intensity is rather weak, initially around 15 cps to 20 cps. The semi-logarithmic plot exhibits a time dependence that can not be described by first-order rate law. The (small) deviation from an exponential decay rate can be attributed to radially varying bleaching rates caused by a spatially varying intensity in the laser focus.

In the presence of the tip, the bleaching time constant drops dramatically, as is evident from Fig. 15 that plots the TER intensity of the 1618 cm^{-1} band vs. time on a semilogarithmic scale. Here again, we observe a deviation of the

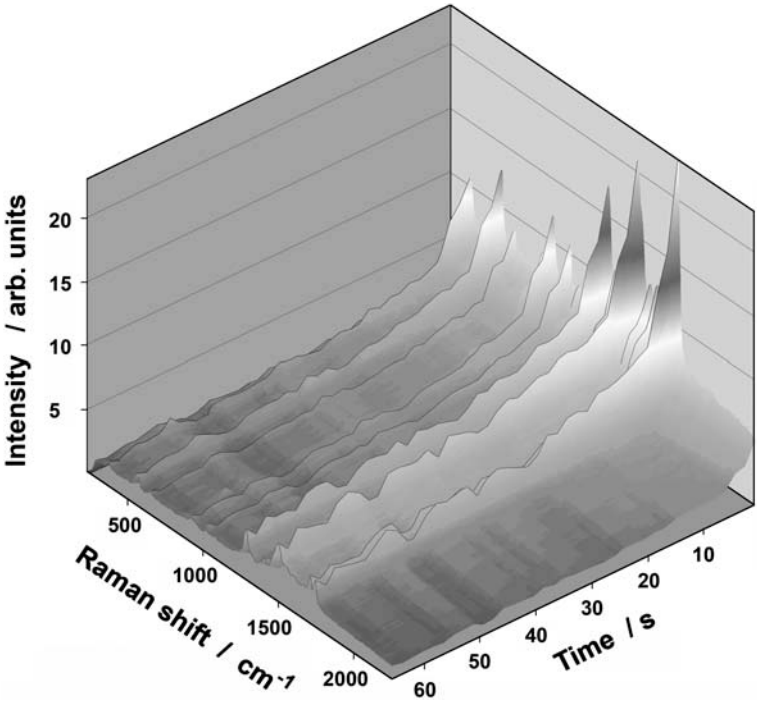

Fig. 13. Three-dimensional plot of the TER intensity of MGITC vs. wave number and time. Laser power: 0.5 mW; acquisition time: 1 s; delay between spectra: 1 s. (Reprinted with permission from [52])

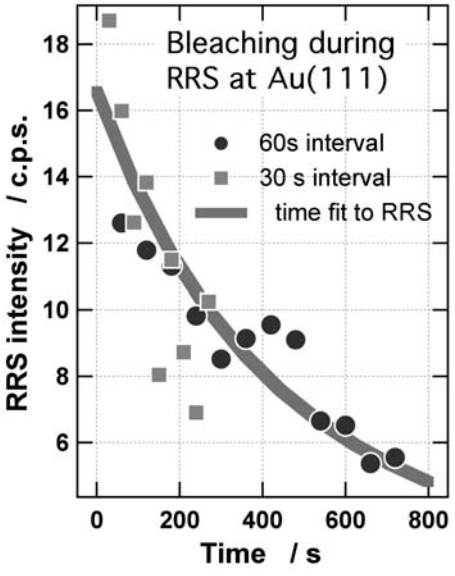

Fig. 14. Time dependence of the RRS signal of MGITC (the 1616 cm^{-1} band) adsorbed on an Au(111) surface. *Filled squares* and circles represent experimental data; the *solid line* is a fit curve using (1). No tip present. Laser power: 5 mW (Reprinted with permission from [52])

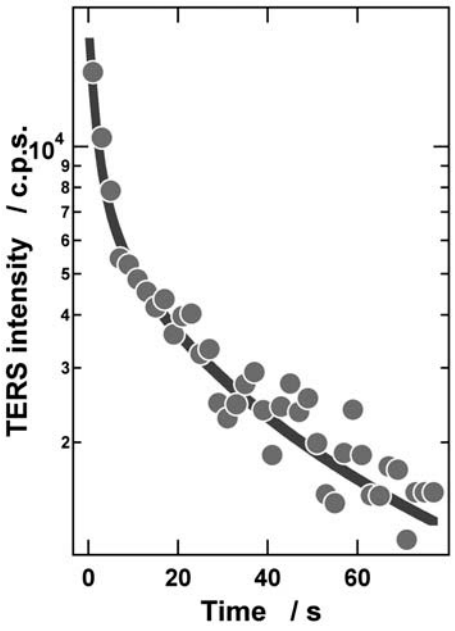

Fig. 15. Time dependence of the TER intensity of the 1618 cm^{-1} band of MGITC adsorbed on an Au(111) surface. *Filled circles* represent experimental data, the *solid line* is a fit curve using (2). Tip in tunneling position. Laser power: 0.5 mW. (Reprinted with permission from [52])

curve from a first-order rate law. For a complete description of the bleaching behavior, two different bleaching processes have to be taken into account, but each of them deviates from a first-order rate law (i.e. following a non-exponential decay). The two bleaching processes are associated with different bleaching constants and amplitudes (initial intensities). Obviously, the bleaching occurs differently for MGITC located in an intact environment (fast) and for MGITC in a disordered/bleached environment (slow). Important here is the initial bleaching process with its short time constant.

The ratio of the bleaching time constants can be related to the square of the field enhancement g^2 [52]. Assuming Gaussian distributions for the incident and enhanced light intensities and different radii R_f (RRS) and R_T (TERS) ($I(r) = I_\mathrm{L}\exp(-r^2/R_\mathrm{f}^2)$ and $g^2(r)I_\mathrm{L} = g_0 I_\mathrm{L}\exp(-r^2/R_\mathrm{T}^2)$, respectively)[8], the bleaching behavior can be given in analytical form:

$$
\begin{aligned}
I_\mathrm{RRS} &\propto N_0 \left(\frac{\mathrm{d}\sigma}{\mathrm{d}\Omega}\right)_\mathrm{RRS} \frac{I_\mathrm{L}}{2}\left(4\pi\int_0^\infty e^{-e^{-r^2/R_\mathrm{f}^2} I_\mathrm{L}\gamma t - r^2/R_f^2} r\,\mathrm{d}r\right) \\
&= N_0 \left(\frac{\mathrm{d}\sigma}{\mathrm{d}\Omega}\right)_\mathrm{RRS} \frac{I_\mathrm{L}}{2} R_f^2 \pi \left[\frac{1}{I_\mathrm{L}\gamma t}\left(1 - e^{-I_\mathrm{L}\gamma t}\right)\right], \qquad (1)
\end{aligned}
$$

[8] This formulation of the bleaching behavior is more stringent than the one given in [52], because the quantities R_f and R_T are here defined as the radii of the focus and of the enhanced intensity underneath the tip that are, in principle, measurable.

$$
\begin{aligned}
I_{\mathrm{TERS}} &\propto N_0 \left(\frac{\mathrm{d}\sigma}{\mathrm{d}\Omega}\right)_{\mathrm{RRS}} g_0^4 \frac{I_{\mathrm{L}}}{2} \left(4\pi \int_0^\infty e^{-e^{-r^2/R_{\mathrm{T}}^2} g_0^2 I_{\mathrm{L}} \gamma t - 2r^2/R_{\mathrm{T}}^2} r \,\mathrm{d}r\right) \\
&= N_0 \left(\frac{\mathrm{d}\sigma}{\mathrm{d}\Omega}\right)_{\mathrm{RRS}} g_0^4 \frac{I_{\mathrm{L}}}{2} 2R_{\mathrm{T}}^2 \pi \\
&\quad \times \left\{ \frac{2}{\left(g_0^2 I_{\mathrm{L}} \gamma t\right)^2} \left[1 - e^{-g_0^2 I_{\mathrm{L}} \gamma t} \left(1 + g_0^2 I_{\mathrm{L}} \gamma t\right)\right] \right\}, \qquad (2)
\end{aligned}
$$

where N_0 is the number of the adsorbates per unit area, $\left(\frac{\mathrm{d}\sigma}{\mathrm{d}\Omega}\right)_{\mathrm{RRS}}$ is the differential (resonance) Raman cross section of the adsorbate, I_{L} is the incident intensity in the center of the laser focus (i.e., twice the average intensity), γ is the bleaching constant, r is the radial coordinate underneath the tip and along the substrate surface, and t is time. Note that the large brackets on the right sight of (1) and (2) represent the time dependences, which are normalized to one for $t \to 0$ or $\gamma \to 0$. The bleaching time constants can be associated with $\tau_{\mathrm{RRS}} = 1/(I_{\mathrm{L}}\gamma)$ and $\tau_{\mathrm{TERS}} = 1/\left[g_0^2(I_{\mathrm{L}}/10)\gamma\right]$, where the divisor takes into account the laser intensity reduced by a factor of 10.[9] Building the ratio of the bleaching time constants, one can express the field enhancement g_0 as

$$
g_0 = \sqrt{\frac{\tau_{\mathrm{RRS}}}{\tau_{\mathrm{TERS}}/10}}\,.
$$

Using (1) and (2) for a fit to the experimental data (gray curves in Fig. 14 and Fig. 15), we obtain: $\tau_{\mathrm{RRS}} = 244\,\mathrm{s}$ and $\tau_{\mathrm{TERS}} = 1.78\,\mathrm{s}$.[10] This leads to $g_0 \approx 37$; thus, the TER enhancement is about $F_{\mathrm{TERS}} \approx 2 \times 10^6$.

Next, taking the ratio of (2) and (1) at $t \to 0$ and equalizing it to the experimentally determined ratio $I_{\mathrm{TERS}}/I_{\mathrm{RRS}} = q$, one gets

$$
R_{\mathrm{T}} = \sqrt{\frac{q}{2}} \frac{R_{\mathrm{f}}}{g_0^2}\,.
$$

Since $q \approx 9200$ [11] and $R_{\mathrm{f}} \approx 1000\,\mathrm{nm}$, we obtain for the radius of the enhanced field $R_{\mathrm{T}} \approx 50\,\mathrm{nm}$. This means that the TERS radius is $R_{\mathrm{TERS}} = \frac{1}{2} R_{\mathrm{T}} \approx 25\,\mathrm{nm}$, which agrees with the experimental findings of $R_{\mathrm{TERS}} \approx R_{\mathrm{tip}}$, i.e., the spatial resolution of TERS lies in the order of the size of the tip.

For a more than million-fold enhancement of Raman scattering by the local increase of the electromagnetic field, vibrational spectroscopy of adsorbates that belong to the class of normal Raman scatterers should be achiev-

[9] In (2), a reduced laser intensity is not considered.

[10] Please note that (1) and (2) describe nonexponential curves. Hence, the time constants must be evaluated from the fits or taken from the tangential lines at the points for $t \to 0$.

[11] For the nonreduced laser power, the TER intensity of the $1618\,\mathrm{cm}^{-1}$ line is about 150 000 cps, i.e., ten times higher than shown in Fig. 15.

able. A simple estimate yields the intensities to be expected: For the Raman intensity one can write

$$I_{\mathrm{NRS}} = N_0 \left(\frac{\mathrm{d}\sigma}{\mathrm{d}\Omega}\right)_{\mathrm{NRS}} \frac{I_{\mathrm{L}}}{2}\eta\,.$$

For an adsorbate density $N_0 = 8 \times 10^{14}\,\mathrm{cm}^{-2}$ (a monolayer of small molecules), a typical differential Raman cross section of small molecules $(\mathrm{d}\sigma/\,\mathrm{d}\Omega)_{\mathrm{NRS}} = 4 \times 10^{-30}\,\mathrm{cm}^2$, an incident power of 0.5 mW at 633 nm at the sample, i.e., of 1.6×10^{15} photons per second, and an overall spectrometer sensitivity of $\eta = 0.0005$, one obtains: $I_{\mathrm{NRS}} \approx 0.025$ cps. In other words, for a monolayer of weak Raman scatterers adsorbed at a smooth surface, the expected count rate is much below 1 cps; such low signals are not detectable. The situation is different in the case of TERS for sufficiently large enhancements. Then, $I_{\mathrm{TERS}} = I_{\mathrm{NRS}}\, g_0^4 R_{\mathrm{T}}^2/R_f^2$. This means the expected TERS intensity is about $I_{\mathrm{TERS}} = 125$ cps; these intensity levels are easy to measure. In fact, TERS is achievable for a number of small molecules adsorbed at smooth Au(111) or other single crystals, as listed in Table 1, together with a rough indication of the height of the TER intensity (very strong, strong, middle,weak: vs, s, m, w) [53].

Table 1. TERS for weak Raman scatterers

Adsorbate	Substrate	TERS intensity level	Refs.
CN^-	Au(111)	w	[33]
Benzenethiol	Au(110)	m	[54]
Benzenethiol	Pt(110)	w	[54]
Mercaptopyridine	Au(111)	m	[54]
ClO_4^-	Au(111)	m	[53]
Adenine	Au(111)	w	[53]
Guanine	Au(111)	w	[53]
Cytosine	Au(111)	w	[53]
Thymine	Au(111)	w	[53]

All listed species, exhibit normal Raman scattering, but adsorbed on a gold(111) or on other single crystals they also exhibit TER scattering under proper experimental conditions. Table 1 indicates that TERS is operative (virtually) for all adsorbates. Besides, the kind of substrate metal does not pose severe restrictions on TERS. All experimental evidence shows that TERS is a more general spectroscopical tool than surface-enhanced Raman spectroscopy (SERS) that has a number of severe limitations concerning the kind of adsorbate, the substrates that support SERS, and the surface quality

(roughness is required). Moreover, the TER signals originate from a subwavelength region.

The last few years also saw other very interesting and promising approaches that should be mentioned here briefly. *Ichimura* et al. [55] reported on tip-enhanced coherent anti-Stokes Raman scattering (tip-enhanced CARS or TE-CARS) of a nanometric DNA network structure. The authors used the $1337\,\mathrm{cm}^{-1}$ diazole ring-breathing mode of adenine molecules to record images of DNA nanocrystals at a glass substrate with resolution much beyond the Abbe's diffraction limit [55]. *Keilmann* and *Hillenbrand* [56] developed a microscopy with ultraresolution that is far beyond the limitations of optical microscopy ($< \lambda/10$). Using a tip with radius $< 20\,\mathrm{nm}$, a resolution of $\lambda/60$ was found in the visible and of $\lambda/500$ in the midinfrared wavelength region at $\lambda = 10\,\mu\mathrm{m}$. *Hartschuh* et al. [57] used a metal tip to enhance optical spectroscopy such as two-photon fluorescence or Raman imaging with a resolution better than 20 nm. *Bulgarevich* and *Futamata* [58] built a microscope using confocal epi-illumination/collection optics and an AFM operated in semicontact mode. The authors observed a 1000-fold enhancement of the Raman scattering. *Methani* et al. [59] developed a TERS setup using side illumination optics with the goal of achieving larger enhancement factors and, more importantly, larger imaging contrast. Various molecular, polymeric and semiconducting materials and carbon nanotubes were investigated. *Raschke* et al. [60] used an infrared scattering-type near-field microscope to probe thin films of polymers at a wavelength of $3.39\,\mu\mathrm{m}$ ($2950\,\mathrm{cm}^{-1}$) and with a spatial resolution better than 10 nm. *Billot* et al. [61] focused on an optimized manufacturing of gold tips for TER microscopy and spectroscopy. The authors report on a set of parameters that enable a reproducible production of gold tips with 20 nm radius of curvature. An analogous effort was made by *Saito* et al. [62] for the manufacturing of Ag-coated tips by using a chemical mirror reaction. This leads to a reproducible formation of particles of 40 nm diameter at the tip apex.

Recently, an increased activity in theoretical studies of the optical properties of tip–substrate configurations was noticed. Quite realistic 2D and 3D finite element models were built that include the description of typical tip-sample configurations and geometries in TERS experiments. Huge enhancements for Raman scattering were predicted together with a high spatial resolution [31, 63, 64, 65]. A fruitful, mutual stimulation of experimental and theoretical studies in this rather young scientific field of TERS can be foreseen.

3 Conclusion/Outlook

Tip-enhanced Raman spectroscopy is a vibrational spectroscopy with hitherto unprecedented sensitivity and spatial resolution. Since the enhancement is mainly provided by the near-field excited at the apex of a suitable tip,

TERS appears to be a widely applicable spectroscopy *and* microscopy tool, in contrast to its parents, surface-enhanced Raman spectroscopy (SERS) and scanning near-field optical microscopy (SNOM). TER scattering has been observed for a number of molecules adsorbed at various substrates, including single-crystalline metal surfaces, showing thereby a more than million-fold enhancement of the Raman scattering. It is important to note that the field-enhancement provides, beyond TERS, promising avenues for applications to other optical techniques, such as tip-enhanced CARS, two-photon fluorescence and infrared scattering-type near-field microscopy.

Common to all these approaches is the high spatial resolution that is by far better than Abbe's diffraction limit of $\lambda/2$. The lateral resolution achieved today is in the range of 10 nm to 20 nm. Optical microscopy with such an excellent resolution has a very promising future.

The keys for further advances in the application of enhanced near-fields to scientific and technological (analytical) tasks include the optimization of tips, excitation and collection optics as well as of imaging techniques. Last but not least, it is necessary to achieve a deeper theoretical understanding of the optical properties of the cavity formed between tip and substrate as well as of the influence of (light-absorbing) adsorbates on the optical resonances of this cavity.

Acknowledgements

The author thanks K. F. Domke for carefully reading the manuscript.

References

[1] G. Binning, H. Rohrer, C. Gerber, et al.: Phys. Rev. Lett. **49**, 57 (1982)
[2] P. K. Hansma (Ed.): *Tunneling Spectroscopy: Capabilities, Applications, and New Technologies* (Plenum, New York 1982)
[3] G. Binning, N. Garcia, H. Rohrer: Phys. Rev. B **32**, 1336 (1985)
[4] H. K. Wickramasinghe: Acta Mater **48**, 347 (2000)
[5] B. C. Stipe, M. A. Rezai, W. Ho: Science **280**, 1732 (1998)
[6] J. I. Pascual, J. Gómez-Herrero, D. Sánchez-Portal, et al.: J. Chem. Phys. **117**, 9531 (2002)
[7] K. Kneipp, Y. Wang, H. Kneipp, et al.: Phys. Rev. Lett. **78**, 1667 (1997)
[8] S. M. Nie, S. R. Emory: Science **275**, 1102 (1997)
[9] A. Campion, P. Kambhampati: Chem. Soc. Rev. **27**, 241 (1998)
[10] K. Kneipp, H. Kneipp, I. Itzkan, et al.: Chem. Rev. **99**, 2957 (1999)
[11] A. M. Michaels, J. Jiang, L. Brus: J. Phys. Chem. B **104**, 11965 (2000)
[12] M. Fleischmann, P. J. Hendra, A. J. Mcquillan: Chem. Phys. Lett. **26**, 163 (1974)
[13] D. L. Jeanmaire, R. P. Van Duyne: J. Electroanal. Chem. **84**, 1 (1977)
[14] M. Moskovits, L. L. Tay, J. Yang, T. Haslett: SERS and the single molecule, in V. M. Shalaev (Ed.): *Optical Properties of Nanostructured Random Media* (Springer, Berlin, Heidelberg 2002) pp. 215–226

[15] A. Otto, I. Mrozek, H. Grabhorn, et al.: J. Phys. Condens. Matter **4**, 1143 (1992)
[16] V. M. Shalaev: Optical nonlinearities of fractal composites, in V. M. Shalaev (Ed.): *Optical Properties of Nanostructured Random Media* (Springer, Berlin, Heidelberg 2002) pp. 93–112
[17] V. A. Markel, V. M. Shalaev, P. Zhang, et al.: Phys. Rev. B **59**, 10903 (1999)
[18] M. Moskovits, D. H. Jeong: Chem. Phys. Lett. **397**, 91 (2004)
[19] J. I. Gersten, A. Nitzan: Electromagnetic theory: A spheroidal model, in R. K. Chang, T. E. Furtak (Eds.): *Surface Enhanced Raman Scattering* (Plenum, New York 1982) p. 89
[20] V. M. Shalaev, A. K. Sarychev: Phys. Rev. B **57**, 13265 (1998)
[21] N. Hayazawa, Y. Inouye, Z. Sekhat, et al.: J. Chem. Phys. **117**, 1296 (2002)
[22] R. M. Stöckle, Y. D. Suh, V. Deckert, R. Zenobi: Chem. Phys. Lett. **318**, 131 (2000)
[23] M. S. Anderson: Appl. Phys. Lett. **76**, 3130 (2000)
[24] N. Hayazawa, Y. Inouye, Z. Sekkat, et al.: Opt. Commun. **183**, 333 (2000)
[25] B. Pettinger, G. Picardi, R. Schuster, et al.: Electrochem. Jpn. **68**, 942 (2000)
[26] L. T. Nieman, G. M. Krampert, R. E. Martinez: Rev. Sci. Instrum. **72**, 1691 (2001)
[27] B. Pettinger, G. Picardi, R. Schuster, et al.: Single Molec. **3**, 285 (2002)
[28] A. Hartschuh, E. J. Sanchez, X. S. Xie, et al.: Phys. Rev. Lett. **90**, 95503 (2003)
[29] N. Hayazawa, T. Yano, H. Watanabe, et al.: Chem. Phys. Lett. **376**, 174 (2003)
[30] M. Micic, N. Klymyshyn, Y. D. Suh, et al.: J. Phys. Chem. B **107**, 1574 (2003)
[31] D. Hu, M. Micic, N. Klymyshyn, et al.: Rev. Sci. Instrum. **74**, 3347 (2003)
[32] B. Pettinger, G. Picardi, R. Schuster, et al.: J. Electroanal. Chem. **554**, 293 (2003)
[33] B. Pettinger, B. Ren, G. Picardi, R. Schuster, et al.: Phys. Rev. Lett. **92**, 96101 (2004)
[34] B. Ren, G. Picardi, B. Pettinger: Rev. Sci. Instrum. **75**, 837 (2004)
[35] T. Watanabe, B. Pettinger: Chem. Phys. Lett. **89**, 501 (1982)
[36] K. Kneipp, G. Hinzmann, D. Fassler: Chem. Phys. Lett. **99**, 503 (1983)
[37] K. Kneipp, D. Fassler: Chem. Phys. Lett. **106**, 498 (1984)
[38] B. Pettinger, A. Gerolymatou: Ber. Buns.-Gesellsch. Physik. Chem. **88**, 359 (1984)
[39] B. Pettinger, K. Krischer: J. Electr. Spectrosc. Relat. Phenom. **45**, 133 (1987)
[40] B. Pettinger, K. Krischer, G. Ertl: Chem. Phys. Lett. **151**, 151 (1988)
[41] K. Kneipp, Y. Wang, R. R. Dasari, et al.: Appl. Spectrosc. **49**, 780 (1995)
[42] H. W. Schrötter, H. W. Klöckner: *Raman Spectroscopy of Gases and Liquids* (Springer, Berlin, Heidelberg 1979) p. 123
[43] M. R. Kagan, R. L. McCreery: Langmuir **11**, 4041 (1995)
[44] M. D. Morris, D. J. Wallan: Anal. Chem. **51**, 182 A (1979)
[45] H. X. Xu, J. Aizpurua, M. Kall, et al.: Phys. Rev. E **62**, 4318 (2000)
[46] R. Stöckle, C. Fokas, V. Deckert, et al.: Appl. Phys. Lett. **75**, 160 (1999)
[47] M. S. Anderson, W. T. Pike: Rev. Sci. Instrum. **73**, 1198 (2002)
[48] F. Demming, J. Jersch, K. Dickmann, et al.: Appl. Phys. B **66**, 593 (1998)
[49] D. L. Mills: Phys. Rev. B **65**, 125419 (2002)
[50] R. W. Rendell, D. J. Scalapino, B. Mühlschlegel: Phys. Rev. Lett. **25**, 1746 (1978)

[51] J. Clavilier, R. Faure, G. Guinet, et al.: J. Electroanal. Chem. **107**, 205 (1980)
[52] B. Pettinger, B. Ren, G. Picardi, et al.: J. Raman Spectrosc. **36**, 541 (2005)
[53] D. Zhang, K. F. Domke, B. Pettinger: Chem. Phys. Lett. (to be publ. 2006)
[54] B. Ren, G. Picardi, B. Pettinger, et al.: Angew. Chem. Int. Ed. **44**, 139 (2005)
[55] T. Ichimura, N. Hayazawa, M. Hashimoto, et al.: Phys. Rev. Lett. **92**, 220801 (2004)
[56] F. Keilmann, R. Hillenbrand: Philos. Trans. Roy. Soc. Lond. Ser. A Math. Phys. Eng. Sci. **362**, 787 (2004)
[57] A. Hartschuh, M. R. Beversluis, A. Bouhelier, et al.: Philos. Trans. Roy. Soc. Lond. Ser. A Math. Phys. Eng. Sci. **362**, 807 (2004)
[58] D. S. Bulgarevich, M. Futamata: Appl. Spectrosc. **58**, 757 (2004)
[59] D. Mehtani, N. Lee, R. D. Hartschuh, et al.: J. Raman Spectrosc. **36**, 1068 (2005)
[60] M. B. Raschke, L. Molina, T. Elsaesser, et al.: Chem. Phys. Chem. **6**, 2197 (2005)
[61] L. Billot, L. Berguiga, M. L. De La Chapelle, et al.: Eur. Phys. J. Appl. Phys. **31**, 139 (2005)
[62] Y. Saito, T. Murakami, Y. Inouye, et al.: Chem. Lett. **34**, 920 (2005)
[63] F. Festy, A. Demming, D. Richards: Ultramicroscopy **100**, 437 (2004)
[64] A. L. Demming, F. Festy, D. Richards: J. Chem. Phys. **122**, 184716 (2005)
[65] I. Notingher, A. Elfick: J. Phys. Chem. B **109**, 15699 (2005)
[66] S. Wu, D. L. Mills: Phys. Rev. B **65**, 205420 (2002)

Index